Long Term Effects of Charge Redistribution in Cycled Bias Operating MOS Dosimeter

L. Sambuco Salomone, A. Holmes-Siedle, and A. Faigón

***Abstract*— Techniques based on bias switching during the irradiation allow to extend the measurement range of MOS dosimeters. The response of the REM RFT300 RADFET dosimeter during bias cycled measurements shows a slow shift of the quasi-steady state threshold voltage value during radiation-induced charge neutralization. This phenomenon was previously explained as due to the presence of border traps. In this work, a recently developed numerical model which included the main physical processes leading to hole trapping and neutralization in MOS oxides was used to reproduce this experiment. The application of the model shows that the slow shift of the quasi-steady state threshold voltage during neutralization stages is a consequence of the spatial redistribution of trapped charge within the oxide. The effect this phenomenon has on MOS dosimetry is analyzed.**

***Index Terms*— MOSFETs, radiation effects, solid state detectors.**

I. Introduction

METAL-oxide-semiconductor (MOS) dosimeters are field effect transistors, generally p-channel type, where shift in the threshold voltage (V_t) is used to measure absorbed dose. When the sensor is exposed to radiation, ionization occurs within the gate oxide, and holes are likely to be captured in oxide traps. This positive charge buildup (PCB) is mainly responsible for the V_t shifts.

One of the main drawbacks of MOS dosimetry is the limited dose range of the sensors because of the saturation of the threshold voltage shift. Some techniques were proposed to extend the working life restoring V_t to a predefined value, either by high temperature annealing at 150 °C for 100 hours [1] or Fowler-Nordheim injection of electrons [2]. The measurement range of the dosimeters can be extended through the bias controlled cycled measurement (BCCM) technique [3], in which successive cycles composed of stages of PCB and of radiation-induced charge neutralization (RICN) [4], allow to keep the threshold voltage (V_t) within a predefined window. It was reported that BCCM technique also improves temperature-induced error rejection [5].

Recently, the Fowler-Nordheim injection-based erasing and the BCCM technique were both successfully applied to commercial REM RFT300 RADFET dosimeters [6]. During successive cycles of irradiation with $V_G = 9$ V during PCB and $V_G = 0$ V during RICN, it was observed that the quasi-steady state threshold voltage value at the end of RICN stages slowly shifted towards more negative values as the cycles number increases. This result was first attributed to the presence of border traps, i.e. oxide traps close enough to the Si/SiO_2 interface to make possible tunneling transitions between them and the substrate within the time scale of the measurement [7]. However, a careful modeling of these results leads to a simple and more plausible explanation.

Some heuristic rules were proposed by Fleetwood et al. [8], to predict the response of the device after switching. In this work, a recently developed physics-based numerical model [9] is applied to the above mentioned experimental results. The model deals with the transient problem by solving iteratively the Poisson and continuity equations using known numerical methods. Simulation results provide a physical explanation for the slow steady state V_t shift during RICN stages based on the spatial charge redistribution. The effects the simulation results have on MOS dosimetry are analyzed.

II. Physics-Based Numerical Model

A. Theory

A brief description of the model is provided in this section. For further details, the reader can consult [9].

When radiation interacts with a MOS device, electron-hole pairs (ehp) are generated within the oxide. Only a fraction of them escapes initial recombination. This fractional yield (Y) is strongly dependent on electric field. For ^{60}Co irradiation, Dozier expression is used [10].

The carriers escaping initial recombination flow is driven by the electric field. Field dependent electron mobility is included in the model through an expression that fits Hughes experiments [11]. Holes move dispersively, but at room temperature and usual dose levels, the intrinsic hole mobility can be used [12].

Holes within the oxide can be captured by defects. When an electron is close to a trapped hole, there is a probability of neutralization. Both hole capture and neutralization are treated as proportional to the free carrier density.

Manuscript received June 14, 2016; revised October 8, 2016; accepted November 5, 2016. Date of publication November 8, 2016; date of current version December 14, 2016. This work was supported by ANPCyT and UBA under grants PICT Redes 2007 1907, UBACyT Q025, and REM Oxford Ltd.

L. Sambuco Salomone is with the Laboratorio de Física de Dispositivos-Microelectrónica, INTECIN, Facultad de Ingeniería, Universidad de Buenos Aires, Ciudad Autónoma de Buenos Aires 1063, Argentina (e-mail: lsambuco@fi.uba.ar).

A. Holmes-Siedle is with REM Oxford Ltd., Witney OX29 4PD, U.K.

A. Faigón is with the Laboratorio de Física de Dispositivos-Microelectrónica, INTECIN, Facultad de Ingeniería, Universidad de Buenos Aires, Ciudad Autónoma de Buenos Aires 1063, Argentina and also with the CONICET, Ciudad Autónoma de Buenos Aires 2290, Argentina (e-mail: ahs@radfet.com).

Color versions of one or more of the figures in this paper are available online at http://ieeexplore.ieee.org.

Digital Object Identifier 10.1109/TNS.2016.2626273

0018-9499 © 2016 IEEE. Personal use is permitted, but republication/redistribution requires IEEE permission.
See http://www.ieee.org/publications_standards/publications/rights/index.html for more information.

The system of equations to be solved is the following,

$$\frac{dn_f}{dt} = -\frac{dj_n}{dx} + R_g - R_n n_f p_t \quad (1)$$

$$\frac{dp_f}{dt} = -\frac{dj_p}{dx} + R_g - R_c p_f (P_t - p_t) \quad (2)$$

$$\frac{dp_t}{dt} = R_c p_f (P_t - p_t) - R_n n_f p_t \quad (3)$$

$$\frac{dF}{dx} = -\frac{q}{\varepsilon_{ox}} (p_t + p_f - n_f) \quad (4)$$

n_f and p_f are the densities of free electrons and holes, respectively. p_t is the density of trapped holes, P_t is the density of traps which are considered to be uniformly distributed all over the oxide. R_c and R_n are the trapping and neutralization rates, respectively. The generation rate is $R_g = g_0 Y D_r$, where $g_0 = 8.1 \times 10^{14}$ cm^{-3}Gy^{-1} and D_r is the dose rate. x is referred to the Si/SiO_2 interface. F is the electric field, q is the elementary charge and ε_{ox} is the SiO_2 permitivity ($3.9\varepsilon_0$). The electron (j_n) and hole (j_p) fluxes are described by the usual drift-diffusion model.

The V_t-shift due to changes in the oxide charge is calculated using,

$$\Delta V_t = -\frac{q}{\varepsilon_{ox}} \int_0^{t_{ox}} p_t (t_{ox} - x)\, dx \quad (5)$$

where t_{ox} is the oxide thickness, and free carriers were neglected due to their much lower concentrations relative to the trapped charge.

B. Numerical Implementation

For the numerical simulation of equations (1) – (4), time derivatives were replaced by discretized finite-difference approximations, using the implicit Euler method. This leads to a system of nonlinear equations, which was solved using the full Newton method. In each time step, the iteration ends when the residual of the nonlinear system is lower than a chosen accuracy value. To reduce the condition number of the Jacobian matrix, variables were scaled taking into account the much different order of magnitude of electron and hole mobilities.

For the spatial discretization, the symmetric Franceschetti scheme [13] was implemented to reduce the number of mesh points without compromising the accuracy ($N = 60$, $\theta = 0.08$). Figure 1 shows the mesh, with lines indicating the limits between regions. In order to reduce the computational time, an automatic time step control was employed, based on the local truncation error (LTE).

To avoid numerical instabilities due to the coupling between Poisson and continuity equations, the Scharfetter-Gummel expressions were used to describe the electron and hole fluxes [14]. These expressions were also used at both interfaces as boundary conditions. This approach ensures a smooth transition between low and high field conditions, keeping the correct flux direction for both signs of electric field.

For numerical simulation, capture and neutralization rates are considered fitting parameters for each applied bias.

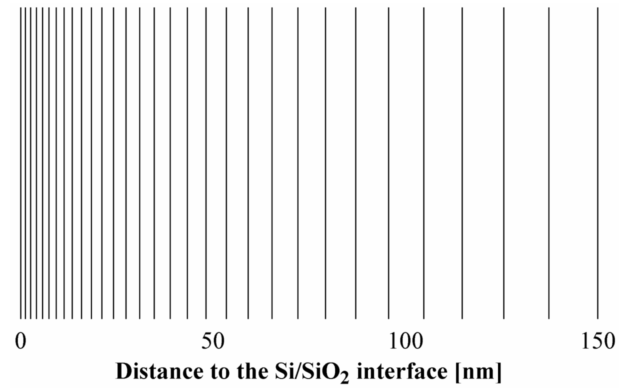

Fig. 1. Spatial mesh used for simulations, according to the Franceschetti scheme with parameters $N = 60$ and $\theta = 0.08$.

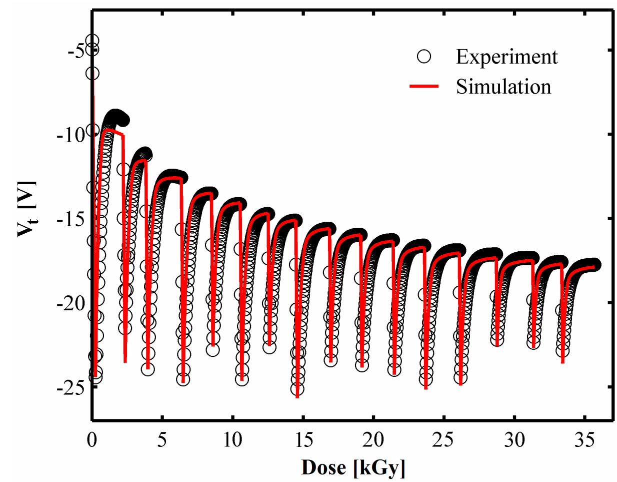

Fig. 2. Experimental (symbols) and simulated (lines) V_t vs. dose curves for 16 successive cycles of PCB at $V_G = 9$ V and RICN at $V_G = 0$ V on a virgin device. $R_C = 10^{-12}$ cm^{-3} during PCB stages and $R_C = 10^{-14}$ cm^{-3} during RICN stages. $R_N = 10^{-9}$ cm^{-3} for all the simulation.

III. Simulation of Experimental Results

The REM RFT300 RADFET dosimeters were exposed to a γ-ray (^{60}Co) source with a high activity. All irradiations were made at room temperature. The experimental details are in [6].

The following parameters were inputs for the model: The SiO_2 thickness $t_{ox} = 300$ nm, the workfunction of aluminium gate $\Phi_{Al} = 4.2$ eV, silicon electron affinity $\chi_{Si} = 4.05$ eV. Resistivity of the phosphorus doped silicon substrate $\rho_{Si} = 4 \pm 1$ Ωcm yields a doping concentration $N_d = (1.2 \pm 0.3) \times 10^{15}$ cm^{-3}. Hole trap density is $P_t = 3 \times 10^{19}$ cm^{-3}.

The first experiment comprised sixteen successive cycles, with a PCB stage with $V_G = 9$ V until V_t reaches -25 V when bias voltage switches to $V_G = 0$ V and the RICN stage begins. V_t rises until a maximum or a quasi-steady value is reached and then switched again. Dose rate was fixed at 6.1 Gy/s. Figure 2 shows V_t vs. dose curve for this measurement. A quite fair agreement was obtained with the numerical model. Capture rate was $R_C = 10^{-12}$ cm^{-3} during PCB stages and $R_C = 10^{-14}$ cm^{-3} during RICN stages, whereas neutralization rate was $R_N = 10^{-9}$ cm^{-3} for all the simulation. The slight inaccuracy in fitting the first cycle was

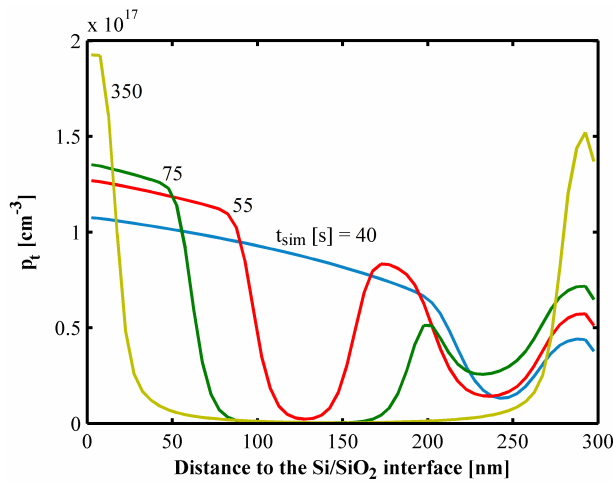

Fig. 3. Spatial distribution of trapped holes within the oxide for different irradiation times (t_{sim}). The curves correspond to the first RICN stage at $V_G = 0$ V. Bias switch occurs at $t_{sim} = 40$ s.

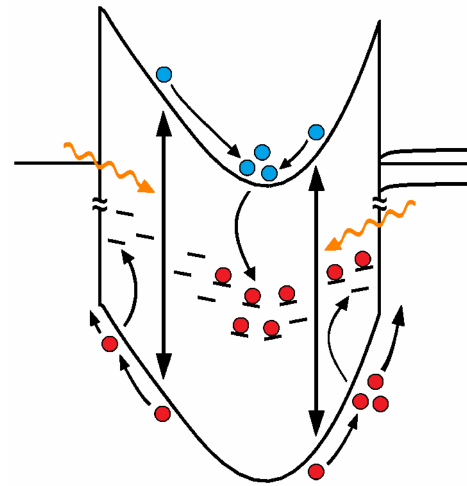

Fig. 4. Band diagram of the MOS structure inmediately after the first bias switch $V_G = 9$ V $\rightarrow$ 0 V.

attributed to our ignorance about the initial state of the oxide charge. During PCB stages V_t shifts to more negative values with an approximately linear response, indicating that for $V_G = 9$ V saturation occurs at much lower values than -25 V. When bias switches to $V_G = 0$ V, charge neutralization occurs, leading to a V_t recovery until the dynamics seems to saturate and even turn-around. The same pattern is repeated in the following cycles but the quasi-steady state V_t value at the end of each RICN stage shifts to more negative voltages. In the original work, it was hypothesized that this was associated with the presence of border traps. However, a simpler physical explanation is provided by the model.

Figure 3 shows the spatial distribution of trapped holes for different times during the first RICN stage. As shown, there are two competing processes: holes trapped far away from the Si/SiO_2 interface are neutralized by electrons while more holes are trapped close to the interface. For short times after bias switches to $V_G = 0$ V, trapped holes neutralization dominates the dynamic, while for long times hole trapping dominates. The origin of this phenomenon is more clear in Fig. 4 when the band diagram of the MOS structure immediately after the switch to $V_G = 0$ V is depicted. As evidenced, a potential well appears within the oxide. Therefore, electrons generated all over the oxide come to the potential well maximizing trapped holes neutralization. At the same time, the presence of the potential well implies that all the holes generated in the substrate side of the potential well are drifted to the Si/SiO_2 interface as occurs during PCB stages. The resulting spatial redistribution of trapped holes as shown in Fig. 3 gives an explanation for the V_t turn-around during a RICN stage.

Figure 5 shows the spatial distribution of electron potential energy within the oxide at the beginning and at the end of first PCB and RICN stages. As shown, hole trapping during the PCB stage enhances the electric field close to the Si/SiO_2 interface whereas it goes to zero far away from it. As bias is switched to $V_G = 0$ V, the potential well is formed. During RICN stage, trapped holes neutralization leads the potential well to dissapear.

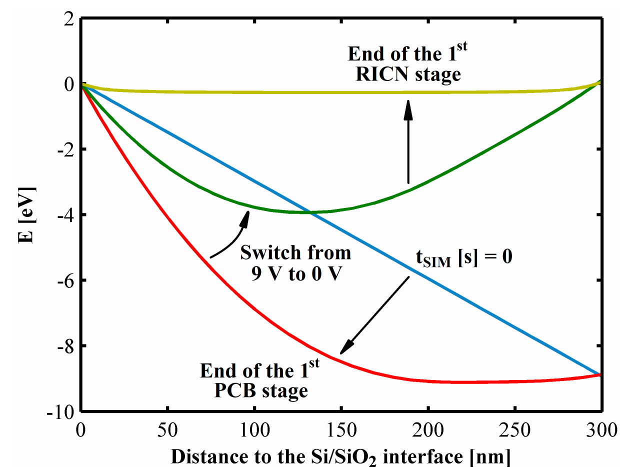

Fig. 5. Spatial distribution of electron potential energy within the oxide at the beginning and at the end of first PCB and RICN stages.

The phenomenon above described also explains the quasi-steady state V_t shift, because once sufficient positive charge was trapped, moderate RICN applied biases leaves the oxide electric field close to the substrate in PCB condition contributing thus in both stages to increase the amount of positive charge trapped close to this interface. Figure 6 shows the spatial distribution of trapped holes at the end of different PCB stages, confirming that holes trapped near the substrate increases with the number of cycles. It is worth to mention that, as the V_t value at the end of PCB stages in Fig. 6 are similar, the increase of trapped holes near the Si/SiO_2 interface is compensated by a decrease of trapped holes far away from this interface, as Fig. 6 clearly shows.

These processes show that the holes trapped near the Si/SiO_2 interface appears as a permanent charge, because the potential well after the bias switch warrants that they are non reachable for free electrons, which are drifted away from both interfaces. To neutralize this positive charge, a sufficiently high negative voltage should be applied to the gate in order to prevent the occurrence of the potential well. A simple

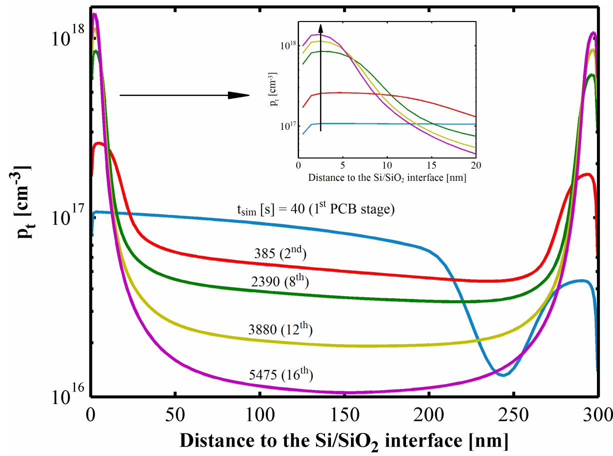

Fig. 6. Spatial distribution of trapped holes within the oxide at the end of different PCB stages at $V_G = 9$ V. The inset shows in detail the first 30 nm.

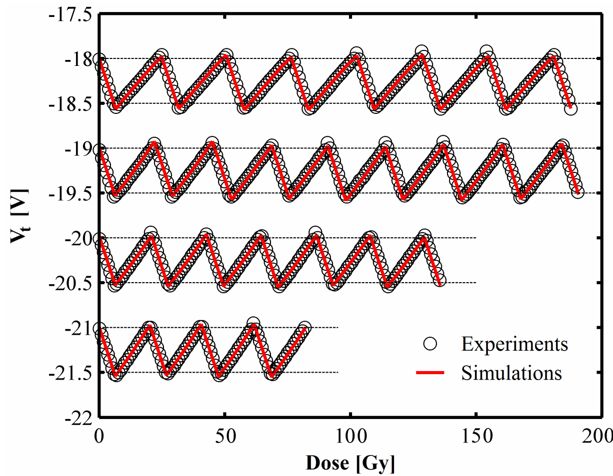

Fig. 7. Experimental (symbols) and simulated (lines) ΔV_t vs. dose curves for BCCM measurements with different windows between −18 V and −21.5 V. Bias voltages during PCB and RICN stages were 9 V and −2 V, respectively.

calculation shows that after the first PCB stage, a bias switch to a voltage lower than $V_G = -20$ V is needed to get a monotonic potential within the oxide from substrate to gate, allowing generated electrons to come to the Si/SiO$_2$ interface.

The BCCM technique was simulated on the RADFET dosimeter with $V_G = 9$ V during PCB stage and $V_G = -2$ V during RICN stage, and compared with experimental results in different 0.5 V V_t-windows in the range between $V_t = -18$ V and $V_t = -21.5$ V (Fig. 7). The model is able to reproduce all the experimental data.

As said in [6], a fairly stable sensitivity during a BCCM measurement is achieved after the device absorbed a high dose level. Figure 8 shows the sensitivity as a function of the V_t value during RICN stages from Fig. 2 for different accumulated doses. As evidenced, all the curves are shifted to lower values of sensitivity as dose increases. In addition, the curves show a linear slope for a wide range of V_t values, and these slopes seems to be very similar, which implies that the decrease in the sensitivity could be interpreted as

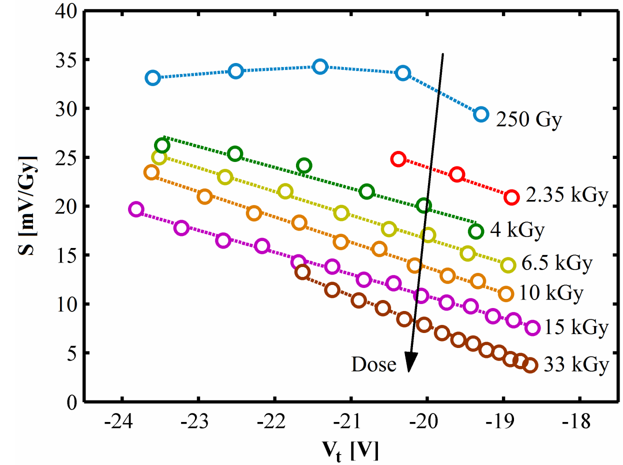

Fig. 8. Sensitivity as a function of V_t value during RICN stages from Fig. 2 for different accumulated doses.

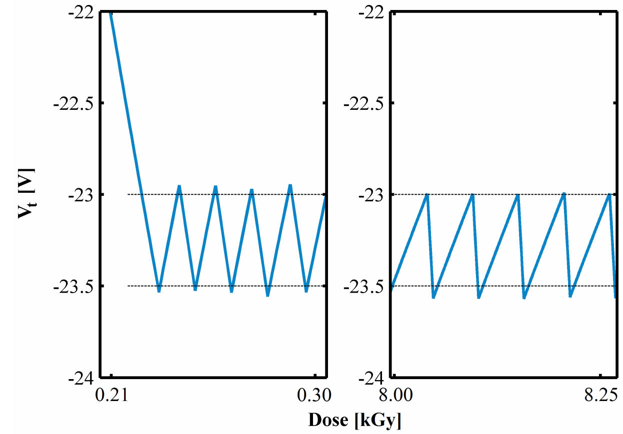

Fig. 9. Simulated response of a RADFET dosimeter under BCCM from a virgin condition with the same bias conditions as in Fig. 2 and a window between $V_t = -23$ V and $V_t = -23.5$ V. The first cycles are shown at left, whereas several cycles after a high accumulated dose are shown at right.

a displacement of the curve towards more negative values following the evolution of the quasi-steady V_t value. In order to deepen this issue, the following simulation was performed: a fresh dosimeter is irradiated with $V_G = 9$ V until the threshold voltage is within the window from $V_t = -23$ V to $V_t = -23.5$ V where a BCCM measurement is simulated with the bias conditions ($V_G = 9$ V for PCB and $V_G = 0$ V for RICN) and the dose level of the experiment of Fig. 2. It comprised about 600 cycles. Figure 9 shows the results of this simulation for several cycles at the beginning (left) and after a high accumulated dose (right). As evidenced, the cycles at right last longer, mainly because of the increase in the RICN stages length. The sensitivity for the PCB stages remains almost constant at $S_{PCB} = 83 \pm 2$ mV/Gy, whereas S_{RICN} goes from 66 mV/Gy down to 9 mV/Gy, as shown in Fig. 10. Also in Fig. 10, the RICN sensitivity at $V_t = -23.5$ V for the curve in Fig. 2 is shown, which decreases slower than that for Fig. 9. This can be explained taking into account that during the BCCM simulation (Fig. 9), (i) the time the device is in PCB mode is larger, and (ii) V_t remains in

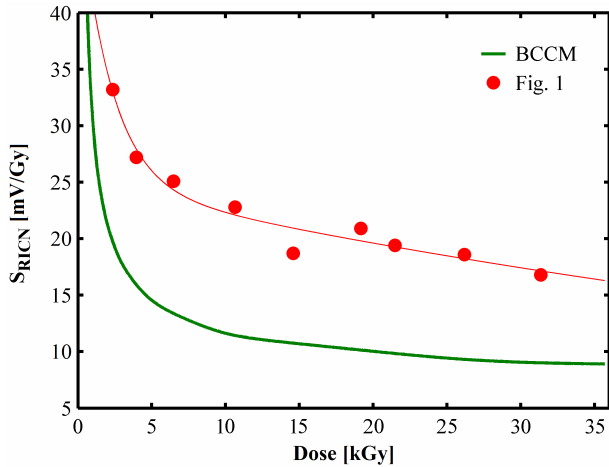

Fig. 10. Sensitivity evolution with dose for RICN at $V_t = -23.5$ V. Solid curve is from BCCM curve in Fig. 9, whereas circles are from Fig. 2 (thin red line is a guide to the eye).

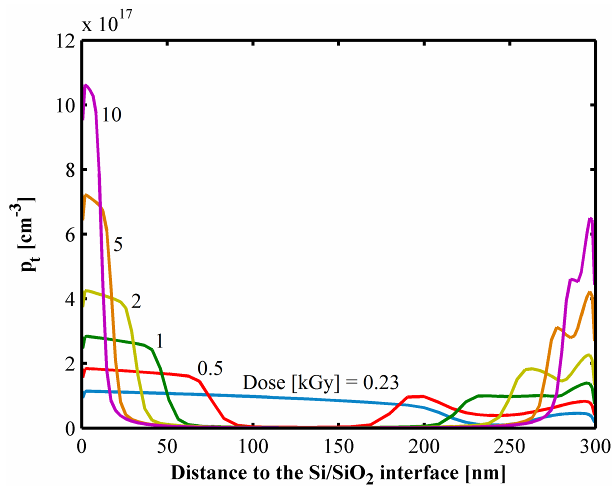

Fig. 11. Spatial distribution of trapped holes within the oxide at the end of PCB stages after different accumulated doses for the simulation shown in Fig. 9.

a window where the RICN sensitivity is maximum. Both facts accelerate the accumulation of trapped positive charge close to the Si/SiO_2 interface, which leads to the change in sensitivity. A RICN measurement at $V_G = 0$ V performed after a higher accumulated dose of 77 kGy shows a sensitivity $S_{RICN} = 10$ mV/Gy [6], consistent with the value predicted by BCCM simulation for high accumulated doses.

To confirm the physical origin of the sensitivity variation, Fig. 11 shows the spatial distribution of trapped holes at the end of different PCB stages. The simulation shows the same trend observed in Figs. 3 and 6, leading to the conclusion that the spatial redistribution of trapped holes is the cause of the sensitivity variation during RICN stages.

IV. Discussion and Conclusions

A recently developed physics-based numerical model was used to simulate the response of REM RFT300 RADFET dosimeters during irradiations under successive cycles comprised of a positive charge buildup (PCB) stage followed by a radiation-induced charge neutralization (RICN) stage. The experimentally observed slow quasi-steady state threshold voltage shift after RICN stages was reproduced through simulations, and this phenomenon was explained as a consequence of trapped charge redistribution within the oxide with a remainder accumulative positive charge close to the interface after each RICN stage. For this to occur, hole traps shall be widely distributed in the oxide, instead of being located in a narrow region close to the Si/SiO_2 interface as usually mentioned in the literature.

It is worthy to note that the same physical phenomenon was observed in 70 nm MOS dosimeters [9]. It suggests this could be a common feature during switched bias irradiations. Related to this charge redistribution is the formation of a potential well immediately after switching to RICN condition. This compels to solve the transient problem instead of using models based on simple analytic equations [15]–[16], or even considering steady fluxes as is usually found in simulation conditions where the transient calculation is unnecessary [17]–[18].

The implications of spatial charge redistribution on BCCM-based MOS dosimetry were analyzed, showing that RICN sensitivity could be affected. It was found from the simulations that the change in sensitivity slows down and seems to saturate after the device is irradiated at tens of kGy. A pre-irradiation with a dose of this order of magnitude would be thus necessary in order to take advantage of the benefits of the BCCM technique. A similar procedure was applied in experimental BCCM measurements performed on different devices [3], in that case justified by the need to saturate interface states generation. The conclusion seems to be that both mechanisms which alter the sensitivity of the BCCM technique on a fresh device, cease with a sufficient pre-irradiation. More experimental results in these dosimeters and in other commercial ones are needed to evaluate the actual impact of charge redistribution on BCCM measurements.

References

[1] A. Kelleher, N. McDonell, B. O'Neill, W. Lane, and L. Adams, "Investigation into the re-use of PMOS dosimeters," *IEEE Trans. Nucl. Sci.*, vol. 41, no. 3, pp. 445–451, Jun. 1994.

[2] J. Lipovetzky, E. G. Redin, and A. Faigón, "Electrically erasable metal–oxide–semiconductor dosimeters," *IEEE Trans. Nucl. Sci.*, vol. 54, no. 4, pp. 1244–1250, Aug. 2007.

[3] A. Faigon, J. Lipovetzky, E. Redin, and G. Krusczenski, "Extension of the measurement range of MOS dosimeters using radiation induced charge neutralization," *IEEE Trans. Nucl. Sci.*, vol. 55, no. 4, pp. 2141–2147, Aug. 2008.

[4] D. M. Fleetwood, "Radiation-induced charge neutralization and interface-trap buildup in MOS devices," *J. Appl. Phys.*, vol. 67, no. 1, pp. 580–583, 1990.

[5] J. Lipovetzky, E. G. Redin, M. A. G. Inza, S. Carbonetto, and A. Faigón, "Reducing measurement uncertainties using bias cycled measurement in MOS dosimetry at different temperatures," *IEEE Trans. Nucl. Sci.*, vol. 57, no. 2, pp. 848–853, Apr. 2010.

[6] J. Lipovetzky, A. Holmes-Siedle, M. Garcia-Inza, S. Carbonetto, E. Redin, and A. Faigón, "New Fowler-Nordheim injection, charge neutralization, and gamma tests on the REM RFT300 RADFET dosimeter," *IEEE Trans. Nucl. Sci.*, vol. 59, no. 6, pp. 3133–3140, Dec. 2012.

[7] D. M. Fleetwood, "Border traps' in MOS devices," *IEEE Trans. Nucl. Sci.*, vol. 39, no. 2, pp. 269–271, Apr. 1992.

[8] D. M. Fleetwood, P. S. Winokur, and L. C. Riewe, "Predicting switched-bias response from steady-state irradiations MOS transistors," *IEEE Trans. Nucl. Sci.*, vol. 37, no. 6, pp. 1806–1817, Dec. 1990.

[9] L. S. Salomone, A. Faigón, and E. G. Redin, "Numerical modeling of MOS dosimeters under switched bias irradiations," *IEEE Trans. Nucl. Sci.*, vol. 62, no. 4, pp. 1665–1673, Aug. 2015.

[10] C. M. Dozier, D. M. Fleetwood, D. B. Brown, and P. S. Winokur, "An evaluation of low-energy X-ray and cobalt-60 irradiations of MOS transistors," *IEEE Trans. Nucl. Sci.*, vol. NS-34, no. 6, pp. 1535–1539, Dec. 1987.

[11] R. C. Hughes, "Hot electrons in SiO_2," *Phys. Rev. Lett.*, vol. 35, no. 7, pp. 449–452, 1975.

[12] R. C. Hughes, "Time-resolved hole transport in α-SiO_2," *Phys. Rev. B*, vol. 15, no. 4, pp. 2012–2020, 1977.

[13] D. R. Franceschetti and J. R. Macdonald, "Numerical analysis of electrical response: Statics and dynamics of space-charge regions at blocking electrodes," *J. Appl. Phys.*, vol. 50, no. 1, pp. 291–302, 1979.

[14] D. L. Scharfetter and H. K. Gummel, "Large-signal analysis of a silicon Read diode oscillator," *IEEE Trans. Electron Devices*, vol. 16, no. 1, pp. 64–77, Jan. 1969.

[15] R. B. Klein, N. S. Saks, and Z. Shanfield, "Saturation of radiation-induced threshold-voltage shifts in thin-oxide MOSFETs at 80 K," *IEEE Trans. Nucl. Sci.*, vol. 37, no. 6, pp. 1690–1695, Dec. 1990.

[16] P. Pavan, R. H. Tu, E. R. Minami, G. Lum, P. K. Ko, and C. Hu, "A complete radiation reliability software simulator," *IEEE Trans. Nucl. Sci.*, vol. 41, no. 6, pp. 2619–2630, Dec. 1994.

[17] H. E. Boesch, F. B. McLean, J. M. Benedetto, J. M. McGarrity, and W. E. Bailey, "Saturation of threshold voltage shift in MOSFET's at high total dose," *IEEE Trans. Nucl. Sci.*, vol. NS-33, no. 6, pp. 1191–1197, Dec. 1986.

[18] R. J. Krantz, L. W. Aukerman, and T. C. Zietlow, "Applied field and total dose dependence of trapped charge buildup in MOS devices," *IEEE Trans. Nucl. Sci.*, vol. NS-35, no. 6, pp. 1196–1201, Dec. 1987.